

Bosonic dark matter halos: excited states and relaxation in the potential of the ground state

Jorge Vicens*

Institut de Ciències del Cosmos, Universitat de Barcelona (IEEC-UB), 08028 Barcelona, Catalonia, Spain

Jordi Salvado†

*Institut de Ciències del Cosmos, Universitat de Barcelona (IEEC-UB), 08028 Barcelona, Catalonia, Spain and
Instituto de Física Corpuscular, València, Spain*

Jordi Miralda-Escudé‡

*Institut de Ciències del Cosmos, Universitat de Barcelona (IEEC-UB), 08028 Barcelona, Catalonia, Spain and
Institució Catalana de Recerca i Estudis Avançats, 08010 Barcelona, Catalonia, Spain*

An ultra-light axion field with mass $\sim 10^{-22}$ eV, also known as wave or fuzzy dark matter, has been proposed as a component of the dark matter in the Universe. We study the evolution of the axion dark matter distribution in the central region of a halo, assuming the mass is dominated by this axion field, and that gravity is the only important interaction. We calculate the excited axion states in the spherical gravitational potential generated by the self-gravitating ground-state, also known as soliton. These excited states are similar to the states of the hydrogen atom with quantum numbers (n, l, m) , here designating oscillation modes of a classical wave. At fixed n , the modes with highest l have the lowest energy because of the extended mass distribution generating the potential. We use an approximate analytical treatment to derive the distribution of mass in these states when a steady-state is reached by dynamical relaxation, and find that a corona with a mass density profile $\rho \propto r^{-5/3}$ should be set up around the central soliton, analogous to the Bahcall-Wolf cusp predicted for the stellar distribution around a central black hole. The central soliton accretes dark matter from the corona as dynamical relaxation proceeds and negative orbital energy flows out. This density profile should remain valid out to the radius where the mass in the corona is comparable to the mass of the central soliton; further than that, the gravitational potential depends on the initial distribution of dark matter and the relaxation time increases rapidly with radius.

I. INTRODUCTION

The nature of dark matter remains one of the most important mysteries in astrophysics and cosmology. The Cold Dark Matter theory (CDM) is able to explain a wide range of observations: the power spectra of the Cosmic Microwave Background fluctuations and large-scale structure distribution of galaxies, the mass distribution in halos of galaxies and clusters that is inferred from velocity distributions [35], X-ray temperatures and gravitational lensing, the total mass density of the Universe and the baryon fraction, the Ly α forest power spectrum, etc. [9, 17]. At the same time, observations on the small-scale distribution of dark matter have indicated possible discrepancies with the predictions of CDM [12, 36, 41], among them the presence of flat cores in the mass density profiles of dwarf galaxies dominated by dark matter [16, 32]. At present there is an on-going debate to understand if these cores, and other possible problems related to the abundance of dwarf satellites [24, 29, 30], can be the result of baryonic processes (involving the formation of stars in the central parts of low-mass dark matter halos, formation of bars and exchange of angular momentum, and the ejection of most baryons in galaxy winds), or if there is an actual discrepancy indicative of a fundamental difference of dark matter from the predictions of CDM.

Several possible alternatives to CDM have been discussed which can modify the predictions on the small-scale structure. For example, Warm Dark Matter proposes that the dark matter particle has just the mass required to give it a primordial velocity dispersion at present that is comparable to the dispersions of dwarf galaxies. This would reduce the abundance of dwarf galaxies and possibly predict cored distributions instead of central cusps [10, 13, 27, 40]. Some of the best lower limits on the CDM particle mass have been obtained from analysis of the Ly α forest power

*Electronic address: j.a.vicens.g@gmail.com

†Electronic address: jsalvado@icc.ub.edu

‡Electronic address: miralda@icc.ub.edu

spectrum [e.g., 5, and references therein].

Ultralight axion dark matter is a general hypothesis first proposed by [18, 20, 34] postulating that the dark matter (or at least part of it) is a scalar or pseudo-scalar field with a very small mass term, implying characteristic wavelengths on galactic scales. The basic idea is that the dark matter is a wave that obeys the equation of a scalar field ψ evolving in a gravitational potential V . The gravitational potential is at the same time determined by the distribution of mass, which is dominated by the dark matter itself except when baryons become more important in central regions of halos due to dissipative processes. To understand the behavior of these dark matter waves, it is generally useful to find eigenstate solutions of the time evolution equation of the field. In the non-relativistic limit (which we generally assume here as an excellent approximation to any galactic dynamic situation far from black hole horizons), the equation for eigenstates of ψ is

$$-\frac{\lambda_a^2}{2}\nabla^2\psi + \frac{V}{c^2}\psi = \frac{i\lambda_a}{c}\frac{\partial\psi}{\partial t} = \frac{\epsilon}{c^2}\psi, \quad (1)$$

where ϵ is an eigenvalue that is the energy per unit mass of the field, and $\lambda_a = \hbar/(m_a c)$ is the reduced Compton wavelength, related to the particle mass m_a of the scalar field. This is the Schrödinger equation for a particle of mass m_a moving in a potential V . When expressed in terms of the wavelength λ_a , equation 1 describes the evolution of the field ψ as a purely classical wave, and there is no reference to the Planck constant. The relation to quantum physics appears only if we insist in relating the field to single particles of mass m_a . In astrophysical situations, the number of particles per stationary state, or occupation number, is extremely large, and the field ψ behaves according to classical physics. However, many of the concepts and terminology from quantum mechanics that are familiar from the study of atomic physics are often useful for describing the phenomenology that this equation gives rise to.

When the only interaction that this scalar field is subject to is gravity, and we assume that this scalar dark matter is the only important mass that is present (neglecting any contribution from baryons or other components), the gravitational potential is given by the Poisson equation with a mass density generated by the field,

$$\nabla^2 V(r) = 4\pi GM|\psi(r)|^2, \quad (2)$$

where the integral of $|\psi|^2$ over all volume is normalized to unity, and M is the total mass of the system. The combination of these two equations is referred to as the *Schrödinger-Poisson* equation.

When looking for eigenstates of these equations, one finds first the solution of the ground state, in which a total mass M of axions forms a self-gravitating object with the lowest possible energy. This solution was first found in [37], giving it the name of a *boson star*. The name was not very appropriate, because stars in astrophysics do not refer to any kind of self-gravitating objects, but to baryonic ones that have produced energy in their interiors through nuclear fusion reactions (brown dwarfs can be considered stars if we include the small amount of initial deuterium burning in these reactions). At the same time, numerical simulations of the evolution of a scalar field [38, 39] that directly solve the Schrödinger-Poisson equation with numerical techniques have identified the formation of collapsed objects and designated them as *solitons* [28]. This has perhaps obscured the fact that the collapsed, stationary objects that form when a random initial scalar field is numerically evolved are the same solution that was found by [37], except that they are surrounded by a dark matter halo that is not part of the stationary solution. In this ground state solution, a mass M of the axion field is confined to a radius R corresponding to a virialized halo with velocity dispersion $v^2 \sim GM/R$, which is equal to the de Broglie wavelength $R \sim \lambda_a c/v \sim \lambda_a c(R/GM)^{1/2}$, implying that $R \sim \lambda_a^2/R_g$, where $R_g = GM/c^2$ is half the Schwarzschild radius of the mass M [26]. At fixed mass M , the object cannot collapse to a smaller radius than this ground state because the increased kinetic energy required to further confine the scalar wave is more than the gravitational energy obtained from the collapse. We shall also refer to these equilibrium self-gravitating objects as scalar field *solitons*.

Apart from the ground state or soliton solution, one can find other stationary states of the coupled Schrödinger-Poisson equation, representing excited states that are also stationary. These states can be easily computed if spherical symmetry is imposed, and have been presented previously (e.g., [6, 21]). These excited states are, however, not physically very meaningful: they represent a solution in which all the axions (or all the energy of the classical axion field) are in an excited state, and the ground state is empty. In practice there would never be any reason why the ground state should be empty. In an evolving classical situation, any small time variation of the potential due to a small part of the axion field being in different states would cause transitions from one eigenstate to all others. If we consider the quantum mechanical case with individual axions, even if all the axions are initially placed in one excited state, there would always be a spontaneous decay rate, however small, to lower energy states, and stimulated decay would subsequently increase exponentially with time as more axions occupy other states.

In this paper we consider a different set of eigenstates that are of greater use to understand the evolution of the classical scalar field under a broad range of conditions: we assume that most of the mass of the axion field is in the ground state, and that a small fraction is in other excited states. We then approximate the gravitational potential V

as being the one created by the axion mass distribution in the ground state, and calculate the excited eigenstates in this fixed potential. The small contribution to the gravitational potential from the mass in the excited states can then be considered as a perturbation that causes small transition rates among the various excited states. These transition rates can be considered as a perturbation expansion for the evolution of a classical field, but also correspond in the usual quantum language to the gravitational scattering of two axions from two incoming to two outgoing states.

The phenomenology of ultra light axion dark matter has been studied in the context of large-scale precision cosmology [19], using astrophysical probes such as the Ly α forest [22], pulsars [8, 14, 23], gravitational waves [15], and laboratory based experiments [1, 11, 25]. Although some constraints can be set in some parts of the parameter space, a conclusive answer has yet to be found. In particular, models in which ultralight axions constitute only a fraction of the dark matter, with other components providing small-scale power, can probably circumvent the difficulties in trying to satisfy observational constraints from dwarf galaxy mass profiles and the Ly α forest at the same time.

We present in section II the solutions to these excited states. Then, in section III we describe an application for the relaxation process of axion dark matter in a spherical distribution around the ground state, and we give an approximate solution to the way these excited states are populated when this relaxation occurs. We conclude in section IV discussing this application as a prediction for the dark matter distribution in various galaxies in the axion dark matter model, and future directions for improving this calculation.

II. EXCITED STATES IN THE POTENTIAL OF THE BOSONIC GROUND STATE

A. The ground state solution

Following the mathematical treatment in [6], and similarly in [37], we apply a re-scaling of the physical variables of our equations to make them dimensionless,

$$r \rightarrow \left(\frac{\hbar^2}{GMm_a^2} \right) = \frac{\lambda_a^2}{R_g} r, \quad (3)$$

$$\psi \rightarrow \left(\frac{\hbar^2}{GMm_a^2} \right)^{-3/2} \psi = \left(\frac{\lambda_a^2}{R_g} \right)^{-3/2} \psi, \quad (4)$$

$$V \rightarrow \left(\frac{G^2 M^2 m_a^2}{\hbar^2} \right) V = \frac{c^2 R_g^2}{\lambda_a^2} V, \quad (5)$$

$$\epsilon \rightarrow \frac{c^2 R_g^2}{\lambda_a^2} \epsilon, \quad (6)$$

where $R_g = GM/c^2$. With this transformation, equations 1 and 2 can be written as,

$$\left(\frac{1}{2} \nabla^2 - V_\alpha \right) \psi_\alpha = \epsilon_\alpha \psi_\alpha, \quad (7)$$

and

$$\nabla^2 V = 4\pi |\psi_\alpha|^2, \quad (8)$$

where the subindex α labels the eigenstate solutions with eigenvalues ϵ_α .

The ground state solution ψ_1 is spherically symmetric [31], so it is solved by replacing $\nabla^2 \psi_1 = (1/r) \partial^2 / \partial r^2 (r \psi_1)$. We use the numerical method described in [6] to convert the differential equations to second-order finite difference equations with two-point boundary conditions requiring the wave function to go to zero at infinity and its derivative to go to zero at the origin. We reproduce the solution found by [37] in figure 1a and 1b, showing the ground state wave function and the corresponding potential in terms of the dimensionless quantities in equations 3 to 6.

In the second plot, the potential of a point mass with the same mass M as the bosonic ground state is shown for comparison. The solution for the potential of the point mass is of course the ground state of the non-relativistic hydrogen atom. The only difference in the self-gravitating bosonic object is that the mass is extended, so the potential is less deep in the center and the wave solution is also more extended compared to the hydrogen atom solution.

B. Excited states and energy spectrum

We now compute the stationary solutions for the excited states assuming that the gravitational potential is dominated by the ground state, which we designate as $V_1(r)$ and is fixed. The self-interaction among the excited states

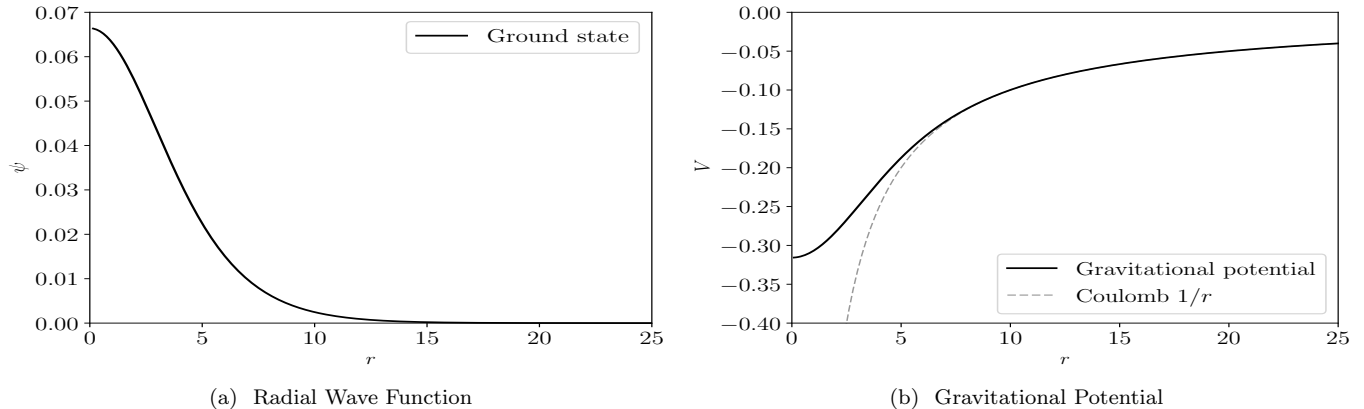


FIG. 1: Numerical solutions for self-gravitating ground state wave function and gravitational potential. The result is shown in terms of the dimensionless magnitudes shown in equations 3 to 6.

is neglected, so can also solve for the states that are not spherically symmetric preserving the spherical symmetry of the equation. The solutions are, as known from atomic physics, the spherical harmonic functions Y_{lm} , times a radial function that obeys the equation

$$\frac{1}{r} \frac{\partial^2 [r\psi_{nl}(r)]}{\partial r^2} + \left(V_1(r) + \frac{l(l+1)}{2m_a r^2} \right) \psi_{nl}(r) = \epsilon_{nl} \psi_{nl}(r), \quad (9)$$

where ϵ_{nl} is the energy eigenvalue of excited state n with angular momentum number l , and $V_1(r)$ is the solution for the ground state potential shown in figure 1b

The wave function numerical solutions for several values of (n, l) are shown in fig. 2. As the principal quantum number n increases, the wave function is more extended with a characteristic half-radius $r \sim n^2$, and the potential of the mass of the ground state is increasingly well approximated as that of a point mass. The eigenfunctions therefore become closer to the hydrogen atom solutions as n increases.

Figure 3 shows the energy eigenvalues that solve the Schrödinger-Poisson equation with the potential $V_1(r)$. The spherically symmetric eigenstates, with $l = 0$, are shown with straight crosses, and the solid line shows the hydrogen atom solution $\epsilon \sim 1/n^2$ for comparison. The spatial extent of the ground state mass flattens the potential and decreases the energy eigenvalues in absolute value, an effect that becomes smaller with growing n . States with angular momentum avoid the central region, and therefore are less affected by the central flattening of the potential and have energies closer to that of the hydrogen atom. The energies ϵ_{nl} increase with l in absolute value at fixed n , contrary to the effect of relativistic corrections in the hydrogen atom (which make the potential steeper than Keplerian, whereas the extended mass makes the potential shallower than Keplerian). Consequently, the lowest energy states in bosonic self-gravitating systems at fixed n are the ones with largest angular momentum. At high n the eigenvalues of different l are increasingly degenerate as the potential approaches that of a point mass.

III. EVOLUTION OF AXION DARK MATTER HALOS UNDER DYNAMICAL RELAXATION

Having established the form of the excited states of bosonic dark matter and their energy spectrum when the gravitational potential is dominated by the ground state, we now consider the way these states are populated when the dark matter is in the process of dynamically relaxing.

A. Relaxation timescale in halos containing axion dark matter

The process of dynamical relaxation can be understood classically as the result of a perturbation on a smooth and time-independent gravitational potential. The scalar field state can be expressed as $\psi = \psi_1 + \psi_e$, where ψ_1 is the ground state and ψ_e is the small contribution of the axions in all the excited states. The gravitational potential has a first order perturbation term in the Laplacian appearing in the Poisson equation that is proportional to $\psi_1 \psi_e^* + \psi_1^* \psi_e$,

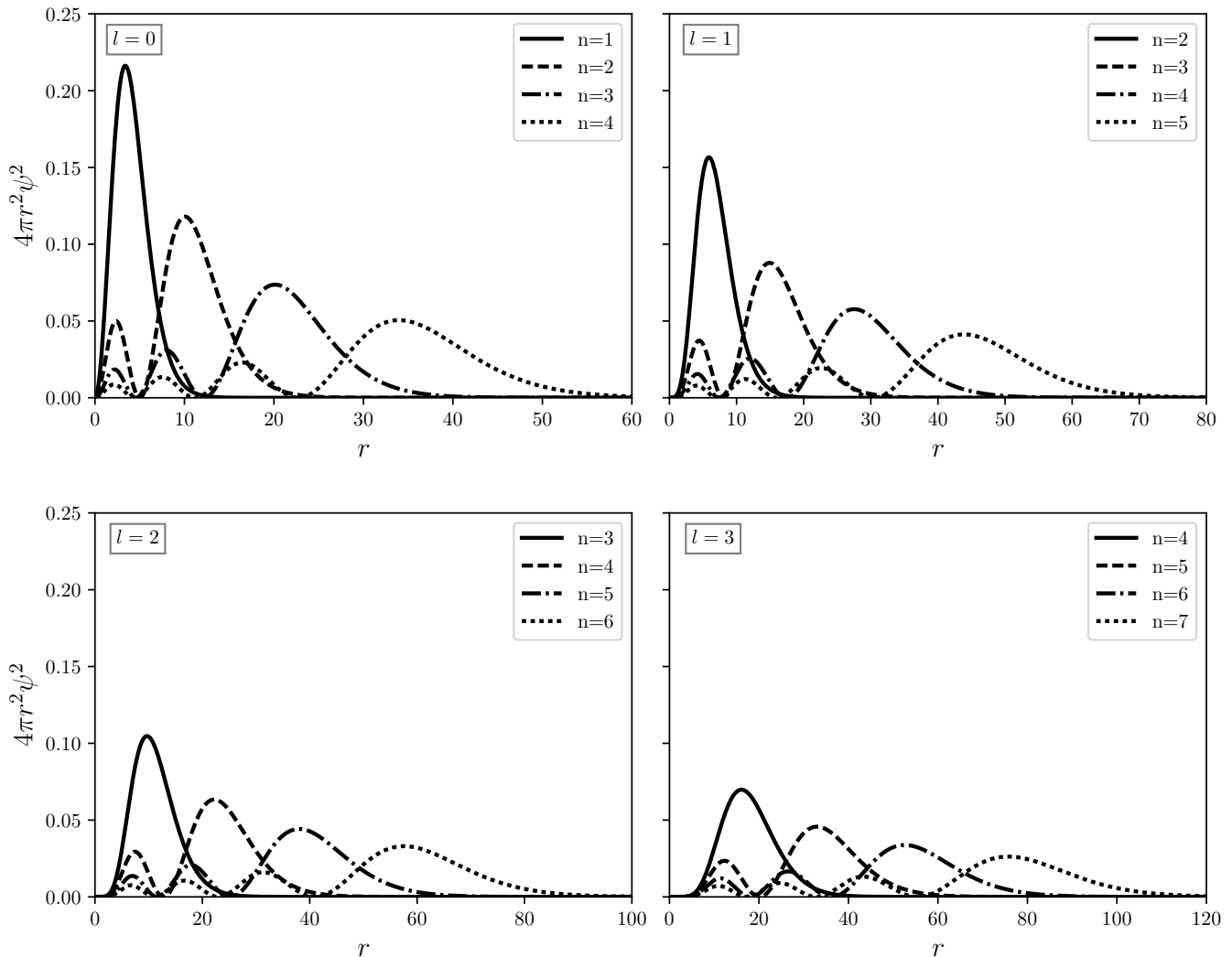


FIG. 2: Numerical solutions for several values of (n, l) for the normalized probability per unit r , $4\pi r^2 \psi^2$, plotted in terms of dimensionless radius.

affecting the evolution of the field. This effect can be expressed as a collisional term in a Boltzmann equation for the evolution of the scalar field amplitude in all the states, where the gravitational interaction of the field in two excited states causes a transition into the ground state and a third excited state, and viceversa. In quantum language, this is understood as the effect of stimulated gravitational scattering of two axions in excited states, into an axion in the ground state and an axion in an excited state that acquires the energy of the two incoming excited axions. The exact quantum transition amplitudes also include the spontaneous scattering rate, but this is negligible when the quantum occupation numbers of all the states are very large, as is the case in all realistic astrophysical situations involving ultralight axions. We note that, in general, axion fields may be subject to self-interactions other than gravity, but here we assume that self-gravity is the only important interaction that induces dynamical relaxation.

Again, we find here that even though the problem we are addressing is one of purely classical waves, the quantum language that has been developed in atomic physics is conceptually useful. The precise method to compute transition rates among excited states induced by this gravitational scattering is to calculate transition amplitudes using Fermi's golden rule, for the process of gravitational scattering of two incoming to two outgoing axions. In this paper, however, we will not carry out this detailed calculation, which we leave for later work. Instead, we limit this work to deriving simple scaling relations for the relaxation time and the implied mass distribution in the excited states. For this purpose, we use the simple rule that the scalar field dynamically relaxes as a collection of quasi-particles that represent the number of independent oscillation modes of the scalar field that exist on a given radial shell around the soliton [21]. In terms of the excited states we have calculated, and for states with $n \gg 1$, the characteristic radial extent of the states

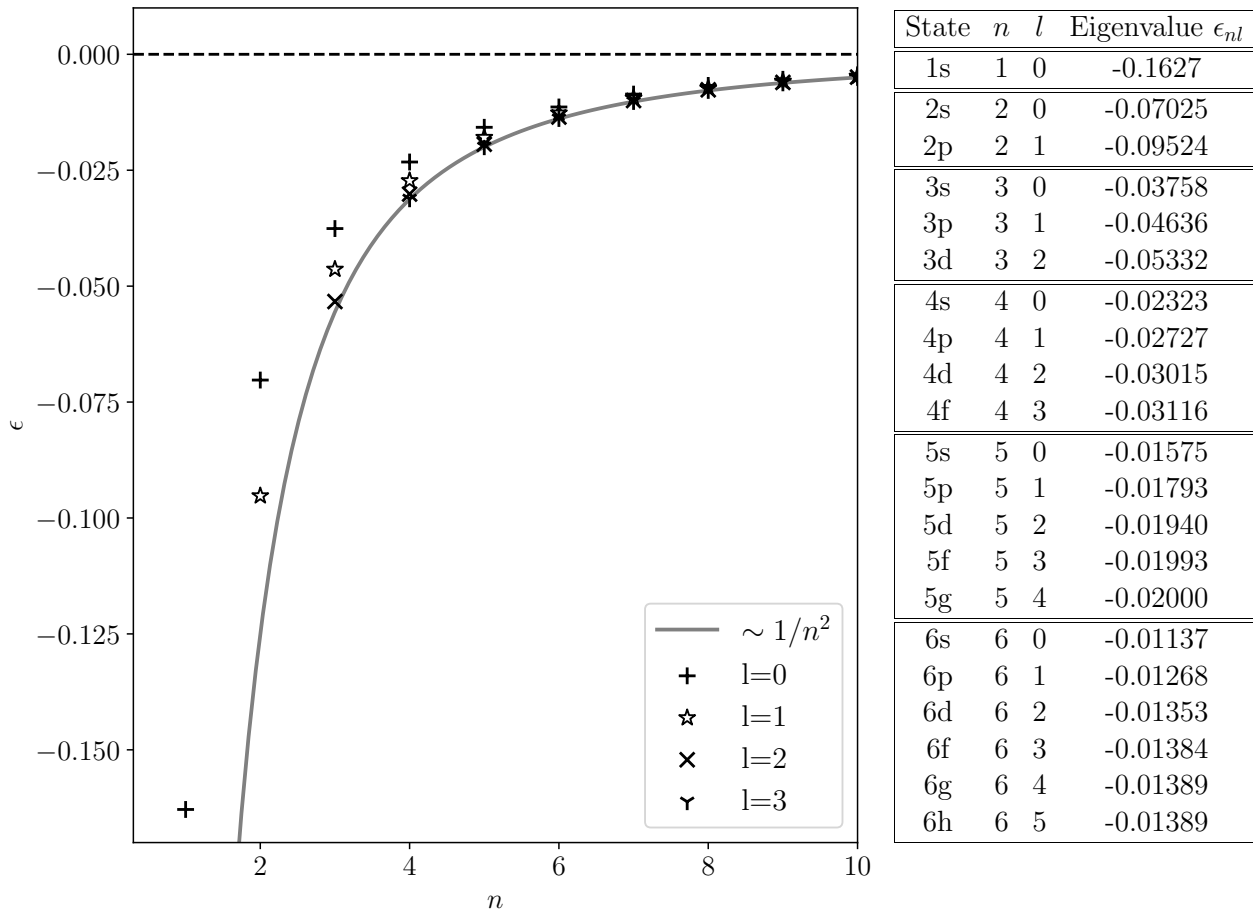


FIG. 3: Energy spectrum of excited states in the potential of the ground state for n up to 10 and all the values $0 < l < n - 1$.

is $r \sim n^2$ (like in the hydrogen atom), and the number of different states up to quantum number n scales as $N_q \sim n^3$, so the number of available states within r scales as $N_q \sim r^{3/2}$. This corresponds to the scaling of the phase-space volume within r of bound orbits in a Keplerian potential, in which the velocity dispersion is $v \sim (GM/r)^{1/2}$ and $(vr)^3 \sim (GMr)^{3/2}$.

Classically, the relaxation time calculated from gravitational scatterings of a system of particles of a fixed mass m and mass density ρ with a velocity dispersion v is [7]:

$$t_{\text{rel}} = 0.34 \frac{v^3}{G^2 m \rho \log \Lambda}, \quad (10)$$

where $\log \Lambda$ is the Coulomb logarithm factor. If the total mass of the system within r that generates the gravitational potential is M , this can be expressed as

$$t_{\text{rel}} \simeq \frac{t_{\text{orb}}}{\log \Lambda} \frac{M}{N_p m} \frac{M}{m}. \quad (11)$$

where N_p is the number of particles within r and $t_{\text{orb}} = r/v$ is the orbital time. This has a simple interpretation: when the particles account for all the mass of the system M , then the relaxation time scales as $N_p t_{\text{orb}}$, and when the particles are only a fraction $f_p = N_p m/M$ of the mass of the system, the relaxation time (at fixed M/m) is increased by the inverse of this fraction because there are fewer particles of mass m available to produce scatterings.

This equation also determines the relaxation time of the scalar field in the potential of a central mass M as a function of the number of quasi-particles, except that now the quasi-particle mass m is not constant but varies with radius depending on the scalar density. The number of quasi-particles, on the other hand, is fixed to the number of excited states of the field available at each radius r .

B. The radial profile of relaxing axion dark matter around the ground state

Let us now recall the derivation of the equilibrium distribution of particles orbiting in a Keplerian potential after they have dynamically relaxed. This problem was addressed to understand the evolution of a star cluster moving in the potential of a central massive black hole, which was predicted to reach a stationary distribution known as the Bahcall-Wolf cusp [2, 3]. We are interested here only in the radial profile shape, so we ignore the slowly varying Coulomb logarithm term. One can first try the assumption that relaxation leads to a flow of particles toward the center of the potential that is constant in radius [33], if stars are simply assumed to disappear once they reach the center and are destroyed by the black hole. In this case we would require N_p/t_{rel} to be constant, corresponding to the assumption that the N_p particles at radius r move to an interior shell after time t_{rel} and that this flow has to be conserved at all radii. This implies (using $t_{\text{orb}} \sim r^{3/2}$ in a Kepler potential)

$$N_p m / t_{\text{rel}} \sim N_p^2 m^3 / M^2 / r^{3/2} \sim \text{constant} , \quad \rho(r) \sim N_p m / r^3 \sim r^{-9/4} . \quad (12)$$

This density profile assumes that the mass flow is locally determined by the relaxation time at each radius. However, the orbital energy of the particles also needs to be conserved and has to flow out radially as particles move in. The steep density profile in 12 does not allow for the orbital energy to flow out fast enough, because the negative energy per particle decreases as $1/r$ in the Keplerian potential. The mass flow is therefore determined by the relaxation time at an outer radius that fixes the rate at which orbital energy can flow out. A constant transfer rate of orbital energy is then the correct assumption, implying

$$N_p m / (r t_{\text{rel}}) \sim N_p^2 m^3 / M^2 / r^{5/2} \sim \text{constant} , \quad \rho(r) \sim N_p m / r^3 \sim r^{-7/4} . \quad (13)$$

We now repeat the same derivation for the system of relaxing quasi-particles of the scalar field. In this case, the scalar wave is exchanging energy among modes as relaxation proceeds, leading to an accretion rate onto the ground state while some of the scalar field is excited to higher energy levels. The assumption of a constant mass flow is again not self-consistent, because even though it would allow for conservation of the scalar field mass as it accretes in a steady-state solution toward the central soliton, it does not provide for a way to absorb the increasing negative potential energy of the scalar field as it moves inward. The scalar field loses orbital energy by scattering some of the axions into higher energy states at larger radius, but just like in the case of classical particles, this occurs only at the relaxation rate. The majority of axions are not scattered into nearly empty, unbound states of axions, but into other populated bound states that also need to transfer their potential energy outwards in radius, so the solution requires a constant outward flow of orbital energy. For quasi-particles, however, their effective mass m_q depends on radius and the number of quasi-particles is determined to evolve radially as $N_q \sim r^{3/2}$, which implies

$$N_q m_q / (r t_{\text{rel}}) \sim N_q^2 m_q^3 / M^2 / r^{5/2} \sim r^{1/2} m_q^3 / M^2 \sim \text{constant} , \quad (14)$$

$$\rho(r) \sim N_q m_q / r^3 \sim r^{-5/3} . \quad (15)$$

In summary, we find that the relaxation of scalar field dark matter in a Keplerian potential determined by the mass of the central soliton should give rise to a corona of scalar dark matter surrounding the soliton, with a mass density profile $\rho \sim r^{-5/3}$, determined by a constant rate of orbital energy flowing out as the dark matter accretes on the soliton. Our derivation neglects the influence of particles or quasi-particles that are ejected after a gravitational encounter at a sufficiently high velocity to become unbound, removing energy from the dynamical system directly, but this should likely be a small contribution because the total relaxation rate is enhanced by the Coulomb logarithm factor.

C. Consequences for density profiles in axion dark matter halos

When a halo made of axion dark matter has been in dynamical equilibrium for a time longer than the central relaxation time t_{rel} , the dark matter should start accumulating in the central ground state or soliton. The mass of

the soliton should increase as more dark matter relaxes, with some mass accreting from the excited states to the soliton and other mass moving to higher energy states. The accretion occurs from a corona of relaxing dark matter surrounding the soliton, with an $r^{-5/3}$ density profile, extending out to a radius r_c at which the mass of the corona is similar to the mass of the soliton. Beyond this radius the gravitational potential is no longer Keplerian, and the dark matter density profile changes and depends on the initial conditions.

The accretion rate of dark matter onto the soliton can be related to the mass of the soliton M_s and the outer radius r_c of the $r^{-5/3}$ corona as follows. The relaxation time at r_c is, from equation 11,

$$t_{\text{rel}}(r_c) \simeq t_{\text{orb}}(r_c) \frac{2M_s}{N_q(r_c)m_q(r_c)} \frac{2M_s}{m_q(r_c)}. \quad (16)$$

We have assumed that the total mass within r_c is $M_s + M_c(r_c) \simeq 2M_s$. The excited states occupying the volume within r_c have quantum number $n_c \simeq (2r_c/r_s)^{1/2}$, where $r_s \simeq 4\lambda_a^2/R_g$ is the half-mass radius of the soliton (see figures 1 and 2 for the approximate factors of 2 and 4 we have introduced). The number of excited states, or quasi-particles, within r_c is $N_q(r_c) \simeq n_c^3/3 \simeq (r_c/r_s)^{3/2}$, and the mass of each quasi-particle is $m_q(r_c) \simeq M_s/N_q(r_c)$. The orbital time at r_c can also be expressed as $t_{\text{orb}}(r_c) \simeq 2^{-1}t_{\text{orb}}(r_s)(r_c/r_s)^{3/2}$, so we finally have

$$t_{\text{rel}}(r_c) \simeq \frac{2}{\log \Lambda} t_{\text{orb}}(r_s) \left(\frac{r_c}{r_s}\right)^3. \quad (17)$$

The timescale required to accrete the mass M_s onto the soliton is, however, much longer than $t_{\text{rel}}(r_c)$. The relaxation process at r_c allows the orbital energy contained in the quasi-particles at r_c to be transported outwards, but the orbital energy per unit mass at r_c is a factor r_s/r_c smaller than at r_s . The timescale for *accretion* of all the mass M_s onto the soliton, t_{acc} , is therefore r_c/r_s times longer than $t_{\text{rel}}(r_c)$:

$$t_{\text{acc}}(r_c) \simeq \frac{2}{\log \Lambda} t_{\text{orb}}(r_s) \left(\frac{r_c}{r_s}\right)^4. \quad (18)$$

We point out again that this accretion timescale assumes that the negative orbital energy that needs to be transported outwards is conducted by means of diffusive gravitational scatterings. Large scatterings that can eject axion streams directly out into unbound orbits are not included, and they may increase the rate of accretion onto the soliton. This effect, however, is also important for the classical stellar dynamics problem of the evolution of a cluster of stars around a massive black hole.

Inside the radius r_c , the relaxation time varies slowly as $t_{\text{rel}} \propto r^{1/3}$. However, outside r_c the relaxation time increases very rapidly with radius. For example, if the dark matter density gives rise to a flat rotation curve as in many galaxies, with a density profile $\rho(r) \propto r^{-2}$, then the orbital time is $t_{\text{orb}} \propto r$, the number of states is $N_q \propto r^3$, and $t_{\text{rel}} \propto t_{\text{orb}}N_q \propto r^4$. The negative orbital energy flowing out therefore accumulates near r_c , pushing out the dark matter and flattening the profile at radius just above r_c .

To find the amount of mass M_s that should have accreted on the central soliton in a dark matter halo after relaxation has started in the center, we solve for the radius r_{cor} that was initially (after the formation of the halo) containing a total mass $2M_s$, and where the accretion time $t_{\text{acc}}(r_{\text{cor}})$ is equal to the halo age. We assume that there are no other mass components (either baryonic or other types of dark matter) that affect the gravitational potential. As illustrating examples, we consider an axion mass $m_a = 10^{-22}$ eV and dark matter halos with the NFW profile [32],

$$\rho(r) = \frac{\rho_0 r_c^3}{r(r+r_c)^2}, \quad (19)$$

with a cusp radius $r_c = 5$ kpc and mass $M_{\text{NFW}} = 10^{10} M_\odot$ within $r_{\text{max}} = 50$ kpc (left panel of figure III C), and a cusp radius $r_c = 18$ kpc and mass $M_{\text{NFW}} = 5 \times 10^{11} M_\odot$ within $r_{\text{max}} = 180$ kpc (right panel in the same figure). The first example represents a dwarf galaxy halo similar to the Large Magellanic Cloud, and the second a galactic halo like that of the Milky Way. Two possible profiles of the axionic soliton and the surrounding $r^{-5/3}$ corona are shown in both panels, with their total mass $2M_s$ indicated next to each curve. The lowest mass soliton in the left panel, with $M_s = 4 \times 10^8 M_\odot$, has a half-mass radius for the soliton $r_s \simeq 4\lambda_a^2/R_g \simeq 0.85$ kpc, where the circular velocity is $v_c(r_s) \simeq 32 \text{ km s}^{-1}$ and the orbital time is $t_{\text{orb}}(r_s) \simeq 2.6 \times 10^7$ yr. The mass $2M_s = 8 \times 10^8 M_\odot$ is contained in the initial NFW profile inside a radius $r_{\text{cor}} \simeq 4.5$ kpc (indicated by the left, blue vertical line), from which the accretion time is $t_{\text{acc}}(r_{\text{cor}}) \sim (r_{\text{cor}}/r_s)^4 t_{\text{orb}}(r_s) \simeq 2 \times 10^{10}$ yr. Therefore, the mass $M_s = 4 \times 10^8 M_\odot$ is roughly the mass that would have been accreted on the soliton at the present age of the Universe. The rate of mass accretion decreases sharply with time: for $M_s = 5 \times 10^8 M_\odot$, the accretion time at $r_{\text{cor}} \simeq 5.3$ kpc increases to $t_{\text{acc}}(r_{\text{cor}}) \sim 6 \times 10^{10}$ yr.

For a halo mass $M_{\text{NFW}} = 5 \times 10^{11} M_\odot$ (right panel), we find that for $M_s = 10^9 M_\odot$, the accretion time at the radius $r_{\text{cor}} = 1.8$ kpc that contains an initial mass $2M_s$ is $t_{\text{acc}}(r_{\text{cor}}) \simeq 3 \times 10^9$ yr, and for $M_s = 1.4 \times 10^9 M_\odot$, we

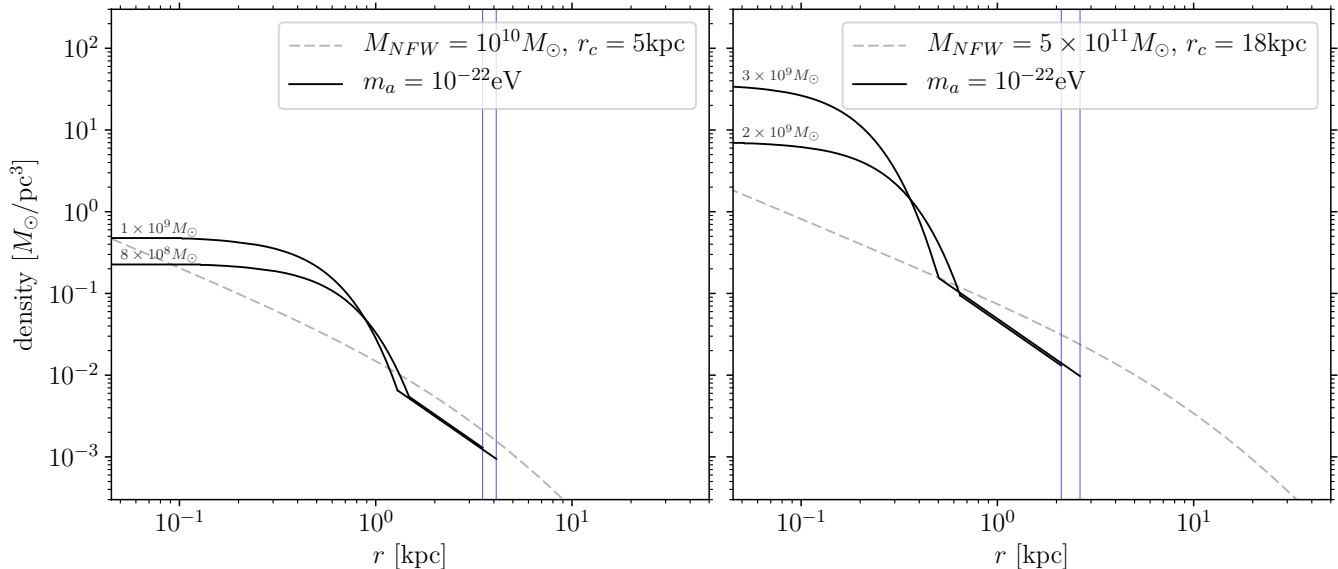


FIG. 4: *Light dashed lines*: Density profile of axion dark matter halos of total mass $M_h = 10^{10} M_\odot$ (left) and $M_h = 5 \times 10^{11} M_\odot$ (right), with the NFW profile and indicated core radii (the total mass is within $r_{max} = 50\text{kpc}$ (left) and $r_{max} = 10\text{kpc}$ (right)). *Solid lines*: Density profile of the soliton and surrounding $r^{-5/3}$ corona, with total masses $2M_s$ indicated in each curve, split in a mass M_s in the soliton and a mass M_s in the corona. Blue vertical lines indicate the radius where the initial NFW profile contains a mass equal to $2M_s$, from which the mass of the soliton and corona have been accreted.

find $r_{cor} = 2.2\text{kpc}$ and $t_{acc}(r_{cor}) \simeq 1.4 \times 10^{10}\text{yr}$. The mass of the soliton increases very slowly with the halo mass and the age, and is strongly dependent on the axion mass m_a and on the presence of baryons or other dark matter components altering the gravitational potential.

IV. DISCUSSION AND CONCLUSIONS

We have presented a numerical calculation of the excited states of a scalar field in the gravitational potential of the mass distribution of the self-gravitating ground state. This solution for the excited states, which approaches the hydrogen atom ones in the limit of large n , is accurate whenever the mass in the ground state is much larger than the combined mass in all the excited states. We have then analytically derived the mass distribution that is expected among all the excited states in a steady-state situation of dynamical relaxation. In this analytical solution, the mass in each excited state is $m_q \propto n^{-1/3} \propto r^{-1/6}$ (where r is the characteristic radius of a state of quantum number n), leading to a density profile of a relaxing corona $\rho \propto N_q m_q / r^3 \propto r^{-5/3}$.

These relaxing coronae should be reproduced by numerical simulations of the evolution of a scalar field starting from cosmological initial conditions, as the ones reported in [38, 39]. Central solitons have indeed been found to form in these type of simulations, but the presence of the surrounding coronae, the accretion rates and the accumulated masses of the solitons predicted by our analytical analysis should be tested. A study of the mass distribution around the solitons along these lines has recently been described in [26].

The formation and growth of these solitons will be strongly influence by the structure of the galaxy that is hosted by the dark matter halo. Our study will therefore have to be generalized to treat the accumulation of scalar dark matter on a soliton in realistic halos with an evolving baryonic mass component. The presence of a central black hole can also affect the mass of the soliton. Relativistic effects near the black hole horizon imply a rate of accretion of scalar dark matter onto the black hole, which might substantially increase the central black hole masses in some galactic nuclei [4].

The presence of these axion dark matter solitons may be testable in the future through a variety of observations, such as detailed mass modeling in the central region of the Milky Way and several dwarf galaxies, and gravitational lensing observations.

Acknowledgments

We are glad to acknowledge useful discussions with Tom Broadhurst, Nick Kaiser, and Helvi Witek. This work was supported in part by Spanish grant AYA2015-71091c and Maria de Maeztu grant MDM-2014-0367 of IC-CUB. J.S. is supported by EU Networks FP10 ITN ELUSIVES (H2020-MSCA-ITN-2015-674896) and INVISIBLES-PLUS (H2020-MSCA-RISE-2015-690575), by MINECO grant FPA2016-76005-C2-1-P, research grant 2017-SGR-929, FPA2014-57816-P and PROMETEOII/2014/050.

-
- [1] Arata Aoki and Jiro Soda. Detecting ultralight axion dark matter wind with laser interferometers. *Int. J. Mod. Phys.*, D26(07):1750063, 2016.
 - [2] J. N. Bahcall and R. A. Wolf. Star distribution around a massive black hole in a globular cluster. *Astrophys. J.*, 209:214–232, October 1976.
 - [3] J. N. Bahcall and R. A. Wolf. The star distribution around a massive black hole in a globular cluster. II Unequal star masses. *Astrophys. J.*, 216:883–907, September 1977.
 - [4] J. Barranco, A. Bernal, J. C. Degollado, A. Diez-Tejedor, M. Megevand, M. Alcubierre, D. Núñez, and O. Sarbach. Schwarzschild Black Holes can Wear Scalar Wigs. *Physical Review Letters*, 109(8):081102, August 2012.
 - [5] Julien Baur, Nathalie Palanque-Delabrouille, Christophe Yèche, Christophe Magneville, and Matteo Viel. Lyman-alpha Forests cool Warm Dark Matter. *JCAP*, 1608(08):012, 2016.
 - [6] David H. Bernstein, Eldar Giladi, and Kingsley R. W. Jones. Eigenstates of the gravitational schrödinger equation. *Modern Physics Letters A*, 13(29):2327–2336, 1998.
 - [7] J. Binney and S. Tremaine. Galactic dynamics. *Princeton, NJ, Princeton University Press*, 747 p., 1987.
 - [8] Diego Blas, Diana Lopez Nacir, and Sergey Sibiryakov. Ultralight Dark Matter Resonates with Binary Pulsars. *Phys. Rev. Lett.*, 118(26):261102, 2017.
 - [9] G. R. Blumenthal, S. M. Faber, J. R. Primack, and M. J. Rees. Formation of galaxies and large-scale structure with cold dark matter. *Nature*, 311:517–525, October 1984.
 - [10] Paul Bode, Jeremiah P. Ostriker, and Neil Turok. Halo formation in warm dark matter models. *Astrophys. J.*, 556:93–107, 2001.
 - [11] Vedran Brdar, Joachim Kopp, Jia Liu, Pascal Prass, and Xiao-Ping Wang. Fuzzy dark matter and nonstandard neutrino interactions. *Phys. Rev.*, D97(4):043001, 2018.
 - [12] J. S. Bullock and M. Boylan-Kolchin. Small-Scale Challenges to the Λ CDM Paradigm. *Ann.Rev.Astron.Astrophys.*, 55:343–387, August 2017.
 - [13] Pedro Colin, Vladimir Avila-Reese, and Octavio Valenzuela. Substructure and halo density profiles in a warm dark matter cosmology. *Astrophys. J.*, 542:622–630, 2000.
 - [14] Ivan de Martino, Tom Broadhurst, S. H. Henry Tye, Tzihong Chiueh, Hsi-Yu Schive, and Ruth Lazkoz. Ultra Light Axionic Dark Matter: Galactic Halos and Implications for Observations with Pulsar Timing Arrays. *Galaxies*, 6(1):10, 2018.
 - [15] P. S. Bhupal Dev, Manfred Lindner, and Sebastian Ohmer. Gravitational waves as a new probe of Bose-Einstein condensate Dark Matter. *Phys. Lett.*, B773:219–224, 2017.
 - [16] John Dubinski and R. G. Carlberg. The Structure of cold dark matter halos. *Astrophys. J.*, 378:496, 1991.
 - [17] C. S. Frenk and S. D. M. White. Dark matter and cosmic structure. *Annalen der Physik*, 524:507–534, October 2012.
 - [18] Jeremy Goodman. Repulsive dark matter. *New Astron.*, 5:103, 2000.
 - [19] Renée Hlozek, Daniel Grin, David J. E. Marsh, and Pedro G. Ferreira. A search for ultralight axions using precision cosmological data. *Phys. Rev.*, D91(10):103512, 2015.
 - [20] Wayne Hu, Rennan Barkana, and Andrei Gruzinov. Cold and fuzzy dark matter. *Phys. Rev. Lett.*, 85:1158–1161, 2000.
 - [21] Hui, Lam and Ostriker, Jeremiah P. and Tremaine, Scott and Witten, Edward. Ultralight scalars as cosmological dark matter. *Phys. Rev.*, D95(4):043541, 2017.
 - [22] Vid Irsic, Matteo Viel, Martin G. Haehnelt, James S. Bolton, and George D. Becker. First constraints on fuzzy dark matter from Lyman- α forest data and hydrodynamical simulations. *Phys. Rev. Lett.*, 119(3):031302, 2017.
 - [23] Andrei Khmelnitsky and Valery Rubakov. Pulsar timing signal from ultralight scalar dark matter. *JCAP*, 1402:019, 2014.
 - [24] Anatoly A. Klypin, Andrey V. Kravtsov, Octavio Valenzuela, and Francisco Prada. Where are the missing Galactic satellites? *Astrophys. J.*, 522:82–92, 1999.
 - [25] Gordan Krnjaic, Pedro A. N. Machado, and Lina Necib. Distorted Neutrino Oscillations From Ultralight Scalar Dark Matter. 2017.
 - [26] Shan-Chang Lin, Hsi-Yu Schive, Shing-Kwong Wong, and Tzihong Chiueh. Self-consistent construction of virialized wave dark matter halos. 2018.
 - [27] Laura Lopez-Honorez, Olga Mena, Sergio Palomares-Ruiz, and Pablo Villanueva-Domingo. Warm dark matter and the ionization history of the Universe. *Phys. Rev.*, D96(10):103539, 2017.
 - [28] David J. E. Marsh and Ana-Roxana Pop. Axion dark matter, solitons and the cusp-core problem. *Mon. Not. Roy. Astron. Soc.*, 451(3):2479–2492, 2015.
 - [29] Alan W. McConnachie. The observed properties of dwarf galaxies in and around the Local Group. *Astron. J.*, 144:4, 2012.

- [30] B. Moore, S. Ghigna, F. Governato, G. Lake, Thomas R. Quinn, J. Stadel, and P. Tozzi. Dark matter substructure within galactic halos. *Astrophys. J.*, 524:L19–L22, 1999.
- [31] I. M. Moroz, Roger Penrose, and P. Tod. Spherically symmetric solutions of the Schrodinger-Newton equations. *Class. Quant. Grav.*, 15:2733–2742, 1998.
- [32] Julio F. Navarro, Carlos S. Frenk, and Simon D. M. White. A Universal density profile from hierarchical clustering. *Astrophys. J.*, 490:493–508, 1997.
- [33] P. J. E. Peebles. Star Distribution Near a Collapsed Object. *Astrophys. J.*, 178:371–376, December 1972.
- [34] P. J. E. Peebles. Fluid dark matter. *Astrophys. J.*, 534:L127, 2000.
- [35] Massimo Persic, Paolo Salucci, and Fulvio Stel. The Universal rotation curve of spiral galaxies: 1. The Dark matter connection. *Mon. Not. Roy. Astron. Soc.*, 281:27, 1996.
- [36] Joel R. Primack. Cosmology: small scale issues revisited. *New J. Phys.*, 11:105029, 2009.
- [37] R. Ruffini and S. Bonazzola. Systems of Self-Gravitating Particles in General Relativity and the Concept of an Equation of State. *Phys. Rev.*, 187:1767–1783, November 1969.
- [38] Hsi-Yu Schive, Tzihong Chiueh, and Tom Broadhurst. Cosmic Structure as the Quantum Interference of a Coherent Dark Wave. *Nature Phys.*, 10:496–499, 2014.
- [39] Hsi-Yu Schive, Ming-Hsuan Liao, Tak-Pong Woo, Shing-Kwong Wong, Tzihong Chiueh, Tom Broadhurst, and W. Y. Pauchy Hwang. Understanding the Core-Halo Relation of Quantum Wave Dark Matter from 3D Simulations. *Phys. Rev. Lett.*, 113(26):261302, 2014.
- [40] Matteo Viel, Julien Lesgourgues, Martin G. Haehnelt, Sabino Matarrese, and Antonio Riotto. Constraining warm dark matter candidates including sterile neutrinos and light gravitinos with WMAP and the Lyman-alpha forest. *Phys. Rev.*, D71:063534, 2005.
- [41] David H. Weinberg, James S. Bullock, Fabio Governato, Rachel Kuzio de Naray, and Annika H. G. Peter. Cold dark matter: controversies on small scales. *Proc. Nat. Acad. Sci.*, 112:12249–12255, 2014. [Proc. Nat. Acad. Sci.112,2249(2015)].